# Light scattering from a small nematic droplet

S. Žumer* and J. W. Doane
*Liquid Crystal Institute, Kent State University, Kent, Ohio 44242*
(Received 15 May 1986)

The scattering matrix, differential cross section, and the total cross section for a small nematic droplet are derived in the Rayleigh-Gans approximation. Different nematic director configurations are considered for the droplet. Those studied are the configurations which result in a spherical droplet from different molecular anchoring angles at the droplet wall. Configurations both in the absence and presence of an applied field are derived and their scattering properties are examined. Some simple cases are treated in detail and the results presented in closed form. In other more practical cases numerical results are presented for the differential and total cross section. Strong dependencies on the impact and scattering angles are found. The possibilities of determining droplet size and nematic director structure from experimental light scattering data are discussed, as well as features relevant to electro-optic light shutters.

## I. INTRODUCTION

Scattering from small droplets is a classical problem extensively studied in the last hundred years. Most studies have been devoted to isotropic objects.[1-3] Besides the well-known Mie solution[4] for a sphere and the more recent solution for the ellipsoid,[5] there are several approximate approaches.[1] The familiar ones are the Rayleigh-Gans approximation (RGA) (Refs. 6 and 7) for small (compared to the wavelength), weak refracting (soft) droplets, the anomalous diffraction approach (ADA) (Ref. 1) for large weakly refracting droplets, and the geometrical optics approach for very large droplets.[1] There are relatively few studied where the optical anisotropy of the droplet material has been taken into account,[2,3] and these are mostly devoted to small objects such as macromolecules[2,8,9] or cases when the symmetry of the optical constants coincides with symmetry of the droplet shape.[10-15]

Materials consisting of a random dispersion of nematic liquid-crystal microdroplets embedded in isotropic solid polymeric media have recently been developed for use in optical and electro-optical devices.[16,17] We present here a theoretical study of the dependence of light scattering on the orientational director configuration in small droplets of nematic liquid crystal. The droplet size which is usually relatively uniform throughout the sample can range between 0.1 to 10 $\mu$m. In most nematic phases the two principal values of the index of refraction $n_e$ and $n_o$ differ by at most 15%.[18] Therefore a nematic droplet in an isotropic medium with an index of refraction $n_m$ approximately equal to $n_e$ or $n_o$ of the liquid crystal represents a "soft" scattering object. It should be stressed that the amount of light scattered by order director fluctuations in a nematic phase is negligible as compared to the amount of light scattered by micron-size droplets. In this contribution we deal only with the submicron droplets where the use of RGA is justified, in which case,

$$|(n_{\mathrm{LC}}/n_m-1)| \ll 1 , \tag{1}$$

where $n_{\mathrm{LC}}$ is neither $n_o$ or $n_e$; and also the maximum phase shift induced by a diametral crossing of a droplet is small,

$$2kR\,|(n_{\mathrm{LC}}/n_m-1)| \ll 1 . \tag{2}$$

Here $k$ is the wave vector in the medium and $R$ is the radius of the droplet. For light with $\lambda=650$ nm and $n_m=1.5$ the droplet diameter should not exceed 0.3 $\mu$m or even 0.2 $\mu$m if we want a reasonably good description, even for temperatures well below the nematic-isotropic phase transition where $n_{\mathrm{LC}}$ has its largest value.

In Sec. II we calculate nematic order director configuration in a spherical droplet for different external fields and different molecular anchoring angles on rigid spherical boundaries. In Sec. III we derive in the RGA the corresponding scattering matrix, the differential cross section, and the total cross section. In Sec. IV some simple cases will be treated in detail. In Sec. V numerical results for scattering patterns and cross sections are presented. The possibilities for determining droplet size and nematic director structure from a comparison with experimental data are discussed, as are features of significance to electro-optic shutters used in displays or optical processing.

## II. DIRECTOR CONFIGURATION

A nematic liquid crystal confined to a small spherical volume where surface-to-volume ratio is relatively high, exhibits a specific director configuration resulting from an interplay between elastic forces, a possible external field, and surface interactions. In our droplets (larger than 100 nm) surface-induced changes in the value and anisotropy of the nematic order parameter can be neglected.[19] We further will suppose that we are below the critical field for the nematic-isotropic phase transition[20] so that field-induced increases in the nematic order parameter can also be neglected. Therefore a constant nematic orientational order parameter approximation will be used. The nematic director, **n**, configuration is then obtained after minimiza-

 

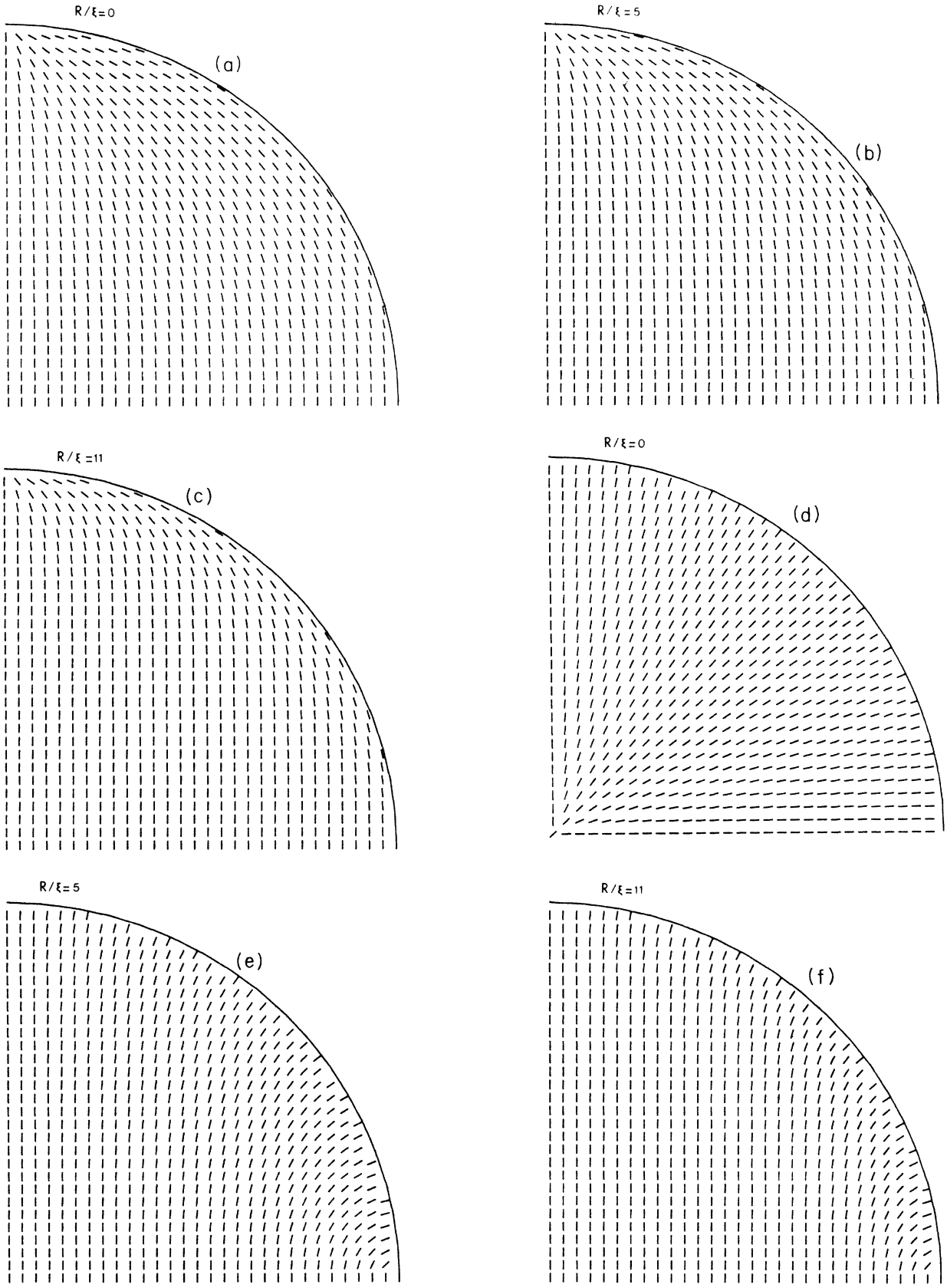


FIG. 1. Schematic representation of the nematic director configurations in a liquid-crystal spherical droplet embedded in a solid for different external fields ($R/\xi=0,5,11$). (a), (b), and (c) correspond to the tangential surface alignment and (d), (e), and (f) to the normal alignment.

tion of the orientational part of the droplet free energy.[21–23] In the case of equal elastic constants ($K_{11}=K_{22}=K_{33}=K$) and strong molecular anchoring on the droplet surface, the free energy of the spherical droplet in an external magnetic field **B** is given by

$$F=\tfrac{1}{2}\int\left[K[(\nabla\cdot\mathbf{n})^2+(\nabla\times\mathbf{n})^2]-\frac{\Delta\chi}{\mu_0}(\mathbf{B}\cdot\mathbf{n})^2\right]dV\,, \tag{3}$$

where the anisotropy of the magnetic susceptibility $\Delta\chi$ is usually positive and typically $\sim 10^{-7}$. Minimization of $F$ results in a partial differential equation which in a cylindrical coordinate system $(\rho,\phi,z)$ has the following form:

$$\nabla^2\theta_n-\left[\frac{1}{\xi^2}+\frac{1}{\rho^2}\right]\cos\theta_n\sin\theta_n=0\,. \tag{4}$$

Here $\theta_n$ stands for the angle between the local director **n** and the direction **N** of the symmetry axis of the director configuration (in further treatment called droplet director). In the presence of the external field **N** is always assumed to be parallel to the field direction. The parameter $\xi$ is the correlation length[24] of the orientational order induced by an infinitely strong anchoring planar surface in a bulk nematic liquid crystal with positive magnetic or electric anisotropy if the preferred orientation induced by the external field is not parallel to that induced by the surface. In the presence of the magnetic field correlation length $\xi$ is given by the well-known relation

$$\xi=\left|\frac{\mu_0 K}{\Delta\chi}\right|^{1/2}\frac{1}{B} \tag{5a}$$

and in an electric field (for insulator regime[24]) by

$$\xi=\left|\frac{K}{\Delta\epsilon\epsilon_0}\right|^{1/2}\frac{1}{E}\,, \tag{5b}$$

where $\Delta\epsilon$ stands for the low-frequency anisotropy of the liquid crystalline dielectric constant. For a typical liquid crystal with $K=4\times10^{-12}$ N, $\Delta\chi=4\times10^{-7}$, $\Delta\epsilon=0.45$, and the correlation length $\xi$ equals 1 $\mu$m, for an electric field $E\simeq1$ V/$\mu$m or magnetic field $B\simeq3.5$ T.

The nonlinear partial differential equation (4) can be solved by the well-known numerical relaxation method. Solutions which can have point or line defects[24] strongly depend on boundary conditions and droplet size. For droplets ($R\gtrsim100$ nm) with tangential molecular alignment on the surface, the bipolar configuration[21] with two boojum-type[25] surface singularities at the poles is characteristic for each value of $\xi$ [see Figs. 1(a), 1(b), and 1(c)].

In a droplet with orthogonal molecular surface anchoring ($R\gtrsim100$ nm), a radial director configuration with a hedgehog-type defect[25] in the center of the droplet is characteristic for $\xi<4$ [see Fig. 1(d)]. At a critical field which corresponds to $\xi\approx4$ there is a phase transition[21] from a structure with a central defect to a structure with an equatorial disclination line. The director configuration in the case of orthogonal surface anchoring in strong fields ($\xi>4$) is illustrated in Figs. 1(e) and 1(f) for two values of the correlation length $\xi$.

## III. RALEIGH-GANS APPROXIMATION

In a droplet surrounded by a medium with an optical frequency dielectric constant $\epsilon_m$ (Fig. 2), the part of the induced polarization $\mathbf{P}_S(\mathbf{r}_m)$ which causes scattering is given by[26]

$$\mathbf{P}_S(\mathbf{r}_n)=\epsilon_0\epsilon_m[\underline{\epsilon}_r(\mathbf{r}_m)-\underline{1}]\mathbf{E}(\mathbf{r}_m)\,, \tag{6}$$

where **E** stands for the local electric field and $\underline{\epsilon}_r$ for the relative (optical frequency) dielectric tensor defined as the ratio $\underline{\epsilon}/\epsilon_m$ between the local dielectric tensor of the liquid crystal $\underline{\epsilon}$ and the dielectric constant of the surrounding medium. In our uniaxial orientational order-parameter approximation the relative dielectric tensor $\underline{\epsilon}_r(r)$ written in its local principal frame

$$\underline{\epsilon}_r=\frac{1}{\epsilon_m}\begin{bmatrix}\epsilon_\perp & 0 & 0\\ 0 & \epsilon_\perp & 0\\ 0 & 0 & \epsilon_{||}\end{bmatrix} \tag{7}$$

is the same everywhere in a droplet where $\epsilon_\perp$ and $\epsilon_{||}$ are eigenvalues of the dielectric tensor $\underline{\epsilon}$. The local direction of the principal axis corresponding to $\epsilon_{||}$ is given by the direction of the nematic director $\mathbf{n}(\mathbf{r}_n)$.

Starting with Maxwell's equations one can easily derive[26] the following exact expression for the scattered electric farfield ($kr\gg1$):[27]

$$\mathbf{E}_s=\mathbf{f}(\mathbf{k},\mathbf{k}')\frac{e^{ikr}}{r}\,, \tag{8}$$

where the scattering amplitude $\mathbf{f}(\mathbf{k},\mathbf{k}')$, is given by

$$\mathbf{f}(\mathbf{k},\mathbf{k}')=-\frac{1}{4\pi}\int\mathbf{k}\times\mathbf{k}'\times\{[\underline{\epsilon}_r(\mathbf{r}_n)-\underline{1}]\cdot\mathbf{E}(\mathbf{k},\mathbf{r}_n)\}\times e^{-i\mathbf{k}'\cdot\mathbf{r}_n}dV\,. \tag{9}$$

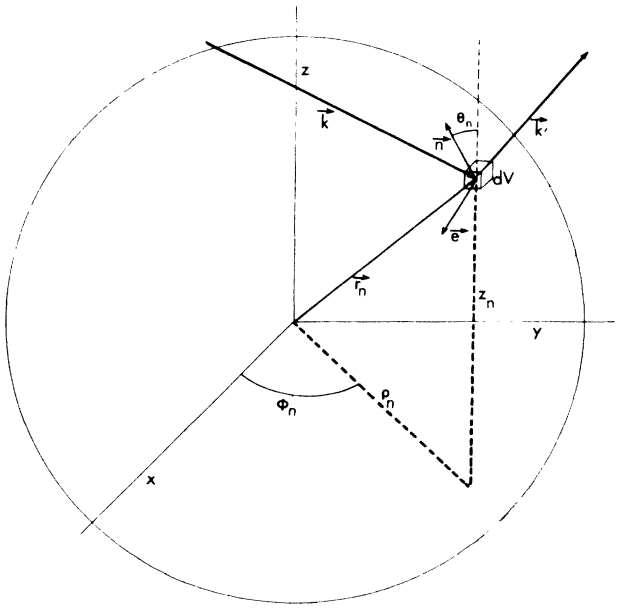


FIG. 2. Schematic representation of the scattering from a droplet defining symbols used in the text.

Here the wave vector $\mathbf{k}$ of the incoming light and $\mathbf{k}'$ of the scattered light (see Fig. 2) have the same magnitude, $2\pi n_m/\lambda$, with $\lambda$ being the wavelength in a vacuum; $n_m=\sqrt{\epsilon_m}$ is the refractive index of the surrounding medium. Unfortunately the internal field $\mathbf{E}(\mathbf{r})$ is unknown. In our case where the condition expressed by Eqs. (1) and (2) are satisfied, the internal field can be well approximated[1,27] by the undisturbed incident plane-wave field,

$$\mathbf{E}(\mathbf{k},\mathbf{r}_n)=\mathbf{E}_0 e^{i\mathbf{k}\cdot\mathbf{r}_n} . \tag{10}$$

This RG approximation is analogous to the well-known Born approximation in quantum mechanics. The scattered farfield is thus the total of dipole radiation emerging from nonuniformly oriented molecules in the droplet. Each dipole is assumed to be excited only by the light from the external source, while the effect of the scattered light from the neighboring molecules and droplets is neglected. If one wants to extend the range of the validity of this approach, correction fields are added to Eq. (10).[28,29] Performing an iteration process one finds that the first correction field can be approximated by the factor $(\epsilon_r-1)(kR)^2E_0/3$ which is much smaller than the incidence field as long as the RGA conditions are satisfied. Here $\epsilon_r$ stands for the average relative dielectric constant,

$$\epsilon_r=\tfrac{1}{3}\mathrm{Tr}(\underline{\epsilon}_r) . \tag{11}$$

Introducing $\mathbf{i}=\mathbf{k}/k$, $\mathbf{i}'=\mathbf{k}'/k$, and the polarization vector $\mathbf{e}=\mathbf{E}_0/E_0$ (see Fig. 3), we can write

$$\mathbf{f}(\mathbf{k},\mathbf{k}')=\frac{1}{4\pi}Vk^2E_0\{\underline{D}\mathbf{e}-\mathbf{i}'[\mathbf{i}'\cdot(\underline{D}\mathbf{e})]\} , \tag{12}$$

where $V$ is the volume of the droplet and

$$\underline{\mathbf{D}}=\frac{1}{V}\int(\underline{\epsilon}_r-\underline{1})e^{-i\mathbf{k}_s\cdot\mathbf{r}_n}dV \tag{13}$$

is in fact a three-dimensional (3D) Fourier transform of $(\underline{\epsilon}_r-\underline{1})$, where $\mathbf{k}_s=\mathbf{k}'-\mathbf{k}$. Separating the isotropic and anisotropic part we can write

$$\underline{\epsilon}_r-\underline{1}=[\underline{1}\zeta+\eta Q(\phi_n,\theta_n)\underline{\beta}_0 Q(\phi_n,\theta_n)^{-1}] , \tag{14}$$

with

$$\zeta=\epsilon_r-1 , \tag{15a}$$

$$\eta=\frac{\epsilon_{\parallel}-\epsilon_{\perp}}{3\epsilon_m} , \tag{15b}$$

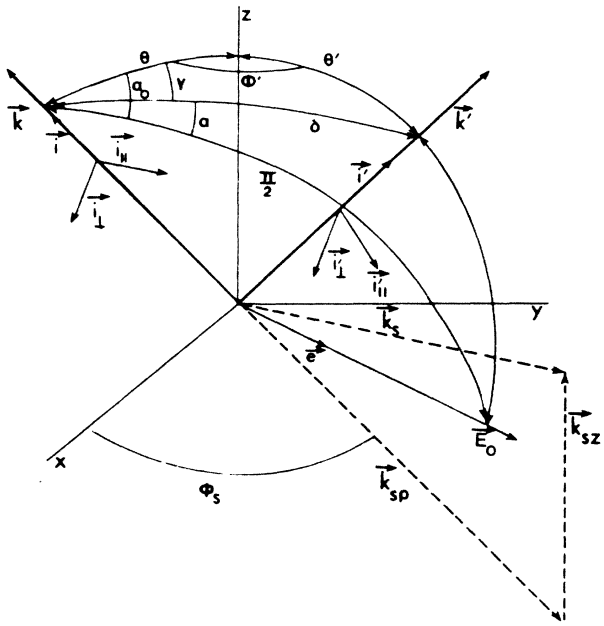


FIG. 3. Schematic representation of the scattering geometry with the notation used in text.

$$\underline{\beta}_0=\begin{bmatrix}1&0&0\\0&1&0\\0&0&2\end{bmatrix} , \tag{16}$$

and where $Q(\phi_n,\theta_n)$ stands for the matrix which transforms from the local frame to the frame fixed to the symmetry axis of the nematic director configuration, i.e., to the direction of the external field if it is present (see Fig. 2). Using Eq. (14) and cylindrical coordinates $(k_{s\rho},\phi_s,k_{sz})$ for the description of the vector $\mathbf{k}_s$, the tensor $\underline{\mathbf{D}}$ given by Eq. (13) can be rewritten in the following form:

$$\underline{\mathbf{D}}=\underline{1}\zeta u(k_sR)+\eta\sum_{j=0,\pm1,\pm2}\underline{\beta}_j v_j(k_{s\rho},\phi_s,k_{sz}) , \tag{17}$$

where

$$\underline{\beta}_{+1}=\begin{bmatrix}0&0&1\\0&0&0\\1&0&0\end{bmatrix},\quad \underline{\beta}_{-1}=-\begin{bmatrix}0&0&0\\0&0&1\\0&1&0\end{bmatrix},$$
$$\underline{\beta}_{+2}=\begin{bmatrix}1&0&0\\0&1&0\\0&0&0\end{bmatrix},\quad \underline{\beta}_{-2}=-\begin{bmatrix}0&1&0\\1&0&0\\0&0&0\end{bmatrix}, \tag{18}$$

and

$$u(k_sR)=\frac{3}{(Rk_s)^3}[\sin(Rk_s)-Rk_s\cos(Rk_s)] , \tag{19a}$$

$$v_0(Rk_{s\rho},Rk_{sz})=\frac{4\pi}{V}\int_0^R\int_0^{\rho(z)}(1-\tfrac{3}{2}\sin^2\theta_n)J_0(k_{s\rho}\rho_n)\cos(k_{sz}z_n)\rho_n\,d\rho_n\,dz_n , \tag{19b}$$

$$v_{\pm1}(Rk_{s\rho},\phi_s,Rk_{sz})=\frac{4\pi}{V}\begin{Bmatrix}\cos\phi_s\\ \sin\phi_s\end{Bmatrix}\int_0^R\int_0^{\rho(z)}\sin(2\theta_n)J_1(k_{s\rho}\rho_n)\sin(k_{sz}z_n)\rho_n\,d\rho_n\,dz_n , \tag{19c}$$

$$v_{\pm 2}(Rk_{s\rho},\phi_s,Rk_{sz})=\frac{4\pi}{V}\begin{Bmatrix}\cos(2\phi_s)\\ \sin(2\phi_s)\end{Bmatrix}\int_0^R\int_0^{\rho(z)}\sin^2\theta_n\,J_2(k_{s\rho}\rho_n)\cos(k_{sz}z_n)\rho_n\,d\rho_n\,dz_n\ . \tag{19d}$$

Here $J_0$, $J_1$, and $J_2$ are Bessel functions. The components of the wave vector $\mathbf{k}_S$ written in terms of angles $\theta$, $\delta$, and $\gamma$ (see Fig. 3) are

$$k_{s\rho}=k\{(1-\cos\delta)[\cos^2\theta(1-\cos\delta)+2(1-\sin\delta\cos\theta\cos\gamma)+(1+\cos\delta)\sin^2\theta\cos^2\gamma]\}^{1/2}\ , \tag{20a}$$

$$k_{sz}=k\,[\cos\theta(1-\cos\delta)-\sin\delta\sin\theta\cos\gamma]\ , \tag{20b}$$

$$\phi_s=\arctan\frac{-\sin\delta\sin\gamma}{\sin\delta\cos\theta\cos\gamma+\sin\theta(1-\cos\delta)}\ , \tag{20c}$$

and its absolute value is given by

$$k_s=2k\sin(\delta/2)\ . \tag{21}$$

It is convenient to decompose the scattered electric field $\mathbf{E}_s$ into a component $(E_s)_{||}$ parallel to the scattering plane defined by vectors $\mathbf{k}$ and $\mathbf{k}'$ and a component $(E_s)_\perp$ orthogonal to this plane which enables us to rewrite Eq. (8) in the following form:

$$\begin{bmatrix}(E_s)_{||}\\ (E_s)_\perp\end{bmatrix}=\frac{Vk^2E_0}{4\pi}\frac{e^{ikr}}{r}\begin{bmatrix}\mathbf{i}_{||}\cdot(\underline{D}\mathbf{e})\\ \mathbf{i}_\perp\cdot(\underline{D}\mathbf{e})\end{bmatrix}\ , \tag{22}$$

where $\mathbf{i}_\perp=\mathbf{i}'_\perp$ and $\mathbf{i}'_{||}$ are unit vectors orthogonal to the direction of the scattered wave vector, perpendicular and parallel to the scattering plane, respectively (see Fig. 4). Introducing a van Hulst scattering matrix $\underline{S}^1$ one can write

$$\begin{bmatrix}(E_s)_{||}\\ (E_s)_\perp\end{bmatrix}=\begin{bmatrix}S_{||||} & S_{||\perp}\\ S_{\perp||} & S_{\perp\perp}\end{bmatrix}\begin{bmatrix}\mathbf{e}\cdot\mathbf{i}_{||}\\ \mathbf{e}\cdot\mathbf{i}_\perp\end{bmatrix}E_0\frac{e^{i\mathbf{k}\cdot\mathbf{r}}}{kr}\ . \tag{23}$$

Here unit vectors $\mathbf{i}_{||}$ and $\mathbf{i}_\perp$ are orthogonal to the direction of the incoming beam. The symbols $||$ and $\perp$ stand for a direction parallel and orthogonal to the scattered plane, respectively (see Fig. 4.) Taking into account $\mathbf{i}_\perp=\mathbf{i}'_\perp$ one can represent the elements of the scattering matrix in the following way:

$$\underline{S}=\frac{Vk^3}{4\pi}\begin{bmatrix}\mathbf{i}'_{||}\cdot(\underline{D}\mathbf{i}_{||}) & \mathbf{i}'_{||}\cdot(\underline{D}\mathbf{i}_\perp)\\ \mathbf{i}_\perp\cdot(\underline{D}\mathbf{i}_{||}) & \mathbf{i}_\perp\cdot(\underline{D}\mathbf{i}_\perp)\end{bmatrix} \tag{24}$$

and more explicitly taking into account the structure of Eq. (17),

$$S_{ps}=\frac{(kR)^3}{3}\left[\zeta(\mathbf{i}'_p\cdot\mathbf{i}_s)u+\eta\sum_j[\mathbf{i}'_p(\underline{\beta}_j\mathbf{i}_s)v_j]\right]\ ,$$

$$p,s=||,\perp\ . \tag{25}$$

The distribution of the scattered light is usually represented by the differential cross section which is defined as

$$\frac{d\sigma}{d\Omega}=\left|\frac{E_s}{E_0}\right|^2r^2\ . \tag{26}$$

Using the previous separation of the scattered field into its $||$ and $\perp$ component, the differential cross section decomposes as well,

$$\frac{d\sigma}{d\Omega}=\left[\frac{d\sigma}{d\Omega}\right]_{||}+\left[\frac{d\sigma}{d\Omega}\right]_\perp\ , \tag{27}$$

where

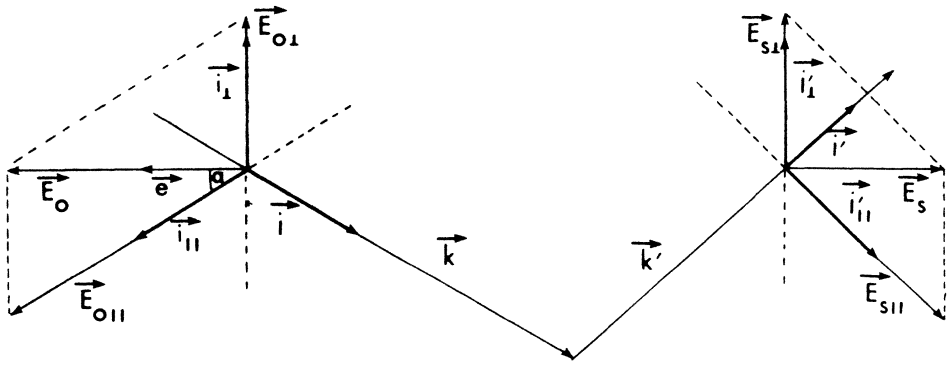


FIG. 4. Schematic representation of the separation of the electric field of the incident and scattered light into parallel $||$ and orthogonal $\perp$ components with respect to the scattering plane.

$$\left.\begin{matrix}\left[\frac{d\sigma}{d\Omega}\right]_{\parallel} \\ \left[\frac{d\sigma}{d\Omega}\right]_{\perp}\end{matrix}\right\} = \frac{\sigma_0}{\pi(kR)^2} \times \begin{cases} |S_{\parallel\parallel}\cos\alpha + S_{\parallel\perp}\sin\alpha|^2 \\ |S_{\perp\parallel}\cos\alpha + S_{\perp\perp}\sin\alpha|^2 \end{cases}$$

$$= \frac{\sigma_0(kR)^4}{9\pi} \times \begin{cases} |\mathbf{i}'_{\parallel}\cdot(\underline{D}\mathbf{e})|^2 \\ |\mathbf{i}'_{\perp}\cdot(\underline{D}\mathbf{e})|^2 . \end{cases} \quad (28)$$

Here $\alpha$ stands for the polarization angle between vectors $\mathbf{i}_{\parallel}$ and $\mathbf{e}$ (see Figs. 3 and 4) and $\sigma_0$ for the geometrical cross section of the droplet. Further, it is worthwhile to write expressions for light intensities measured in a small-angle scattering experiment (SALS).[30,14] There are two common arrangements: *VV* type with incoming polarization parallel to the transmission direction of the analyzer so that the transmitted scattered electric field is

$$(\mathbf{E}_s)_{VV} = \begin{bmatrix}\cos\alpha \\ \sin\alpha\end{bmatrix} \begin{bmatrix} S_{\parallel\parallel} & S_{\parallel\perp} \\ S_{\perp\parallel} & S_{\perp\perp}\end{bmatrix} \begin{bmatrix}\cos\alpha \\ \sin\alpha\end{bmatrix} \frac{E_0}{kr} e^{ikr} , \quad (29)$$

and the corresponding relative intensity

$$I_{VV} = \frac{1}{(kr)^2} |S_{\parallel\parallel}\cos^2\alpha + \tfrac{1}{2}(S_{\parallel\perp} + S_{\perp\parallel})\sin(2\alpha) + S_{\perp\perp}\sin^2\alpha|^2 . \quad (30)$$

*VH* arrangement is where the analyzer is perpendicular to the direction of the polarization of the incoming beam. Here the transmitted electric field of the scattered light is

$$(\mathbf{E}_s)_{VH} = \begin{bmatrix}\sin\alpha \\ -\cos\alpha\end{bmatrix} \underline{S} \begin{bmatrix}\cos\alpha \\ \sin\alpha\end{bmatrix} \frac{E_0}{kr} e^{ikr} , \quad (31)$$

and its relative scattering intensity

$$I_{VH} = \frac{1}{(kr)^2} |S_{\parallel\perp}\sin^2\alpha - S_{\perp\parallel}\cos^2\alpha + (S_{\parallel\parallel} - S_{\perp\perp})\sin\alpha\cos\alpha|^2 . \quad (32)$$

Because of our approximate description of the internal field the optical theorem cannot be used[1] for the evaluation of the total scattered power. The total scattering cross section, therefore, must be calculated simply by an integration of the differential $d\sigma/d\Omega$ cross section over the whole solid angle,

$$\sigma = \int \frac{d\sigma}{d\Omega} d\Omega . \quad (33)$$

In the calculation of the total cross section the separation into $\parallel$ and $\perp$ parts has no use, and we can directly use the following expression for the complete differential cross section:

$$\frac{d\sigma}{d\Omega} = \frac{\sigma_0}{9\pi}(kR)^4 \left\{ \zeta^2[1-(\mathbf{i}'\cdot\mathbf{e})^2]u^2 + 2\eta\zeta u \sum_j v_j[\mathbf{e}\cdot(\underline{\beta}_j\mathbf{e}) - (\mathbf{i}'\cdot\mathbf{e})\mathbf{i}'\cdot(\underline{\beta}_j\mathbf{e})] + \eta^2 \sum_{j,l} v_j v_l \{(\underline{\beta}_j\mathbf{e})\cdot(\underline{\beta}_l\mathbf{e}) - \mathbf{i}'\cdot(\underline{\beta}_j\mathbf{e})[\mathbf{i}'\cdot(\underline{\beta}_l\mathbf{e})]\} \right\} . \quad (34)$$

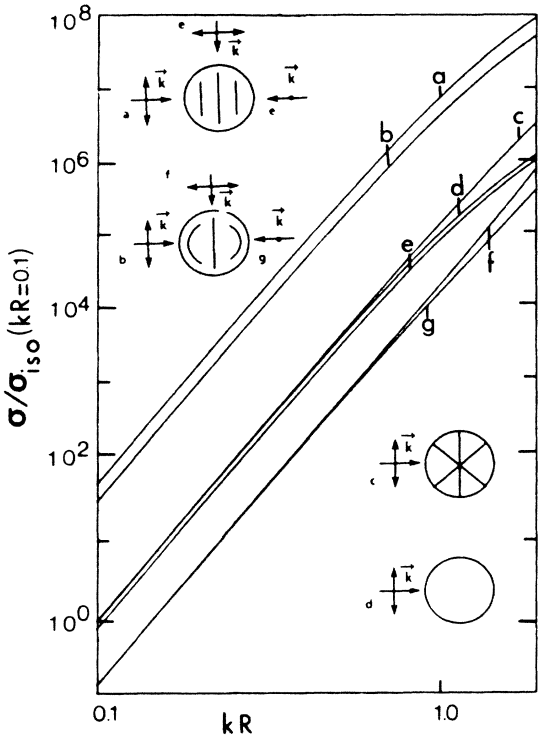


FIG. 5. The $kR$ dependence of the total cross section for the case of: high external field ($R/\xi = \infty$), curve *a* corresponding to $\theta = \pi/2$, $\alpha_0 = 0$ and curve *e* to $\theta = \alpha_0 = 0$ or $\theta = \alpha_0 = \pi/2$; zero external field in the case of tangential surface alignment, curve *b* corresponds to $\theta = \pi/2$, $\alpha_0 = 0$, curve *f* to $\theta = \alpha_0 = 0$, and curve *g* to $\theta = \alpha_0 = \pi/2$; zero external field for the case of normal surface alignment, curve *c*; values $\zeta = 0.04$ and $\eta = 0.08$ were used except in the isotropic case (curve *d*) where $\eta$ is zero.

In general the double integral in Eq. (33) must be performed numerically. Section IV discusses scattering on some previously mentioned nematic structures where simple geometry enables us to simplify the treatment.

## IV. SIMPLE CASES

In some cases symmetry allows us to perform a part of the calculation analytically.

(1). *Radial nematic director configuration.* This case is schematically presented in Fig. 1(d). The dielectric constant is everywhere in the radial direction equal to $\epsilon_{||}$ and to $\epsilon_{\perp}$ in any tangential direction. Such a type of optical anisotropy has been treated already[10,15] and we shall only briefly summarize the results. A properly chosen coordinate system enables us to get $v_{\pm 1}=v_{\pm 2}=0$ and

$$v_0(k_sR)=\frac{3}{(k_sR)^2}\left[4\frac{\sin(k_sR)}{(k_sR)}-\cos(k_sR)-3\,\mathrm{si}(k_sR)\right], \tag{35}$$

where si is the integral sinus. The only two nonzero matrix components are

$$S_{||\,||}=\frac{(kR)^3}{3}[u\zeta\cos\delta+\tfrac{1}{2}(3+\cos\delta)\eta v_0] \tag{36}$$

and

$$S_{\perp\,\perp}=\frac{(kR)^3}{3}(u\zeta-\eta v_0)\,. \tag{37}$$

In agreement with the results of Champion *et al.*,[15] the evaluation of the total cross section reduces to a single numerical integration,

$$\sigma=\sigma_0\frac{(kR)^4}{9}\int\{u^2\zeta^2(1+\cos^2\delta)-2u\zeta\eta v_0(1+\tfrac{3}{2}\cos\delta-\tfrac{1}{2}\cos^2\delta)+\eta^2v_0^2[1+\tfrac{1}{4}(3+\cos\delta)^2]\}d(\cos\delta)\,. \tag{38}$$

(2) *Incident beam parallel to the symmetry axis of the director configuration.* This situation is often realized in optical displays, where an electric field orients droplet directors. In this case only the diagonal components of the scattering matrix are different from zero,

$$S_{||\,||}=\frac{(Rk)^3}{3}\{[\zeta u-\eta(v_0-v_2)]\cos\delta+\eta v_1\sin\delta\} \tag{39a}$$

and

$$S_{\perp\,\perp}=\frac{(Rk)^3}{3}[\zeta u-\eta(v_0+v_2)]\,, \tag{39b}$$

where $v_2=v_{+2}(\phi_s=0)$. Therefore similar diffraction patterns as in previous cases are expected. The resulting differential cross sections

$$\left[\frac{d\sigma}{d\Omega}\right]_{||}=\sigma_0\frac{(kR)^4}{9\pi}\{[\zeta u-\eta(v_0-v_2)]\cos\delta-\eta v_1\sin\delta\}^2\cos^2\alpha\,, \tag{40a}$$

$$\left[\frac{d\sigma}{d\Omega}\right]_{\perp}=\sigma_0\frac{(kR)^4}{9\pi}[\zeta u-\eta(v_0+v_2)]^2\sin^2\alpha\,, \tag{40b}$$

and their sum

$$\frac{d\sigma}{d\Omega}=\sigma_0\frac{(kR)^4}{9\pi}\{[(\zeta u-\eta v_0)^2+\eta^2v_2^2](1-\sin^2\delta\cos^2\alpha)+\eta^2v_1\sin^2\delta\cos^2\alpha$$
$$-2\eta v_2(\zeta u-\eta v_0)(\cos^2\delta\cos^2\alpha-\sin^2\alpha)+\eta v_1(\zeta u-\eta v_0+\eta v_2)\sin(2\delta)\cos^2\alpha\} \tag{41}$$

show twofold symmetry. The same is true for the SALS intensity $I_{VV}$,

$$I_{VV}=\frac{R^2}{9r^2}(kR)^4\,|\,[\zeta u-\eta(v_0+v_2)]\sin^2\alpha+\{[\zeta u-\eta(v_0-v_2)]\cos\delta+\eta v_1\sin\delta\}\cos^2\alpha\,|^2\,, \tag{42a}$$

while the intensity $I_{VH}$ is given by

$$I_{VH}=\frac{R^2}{36r^2}(kR)^4\,|\,[\zeta u-\eta(v_0+v_2)]-[\zeta u-\eta(v_0-v_2)]\cos\delta-\eta v_1\sin\delta\,|^2\sin^2 2\alpha \tag{42b}$$

and shows fourfold symmetry.

Also in this case, the evaluation of the total cross section reduces to a single integration,

$$\sigma=\sigma_0\tfrac{1}{9}(kR)^4\int_{-1}^{1}\{[(\zeta u-\eta v_0)^2+(\eta v_2)^2](1+\cos^2\delta)+\eta v_1(\zeta u-\eta v_0-\eta v_2)\sin(2\delta)$$
$$+[\eta^2v_1^2-2(\zeta u-\eta v_0)\eta v_2]\sin^2\delta\}d(\cos\delta)\,, \tag{43}$$

where $v_0$ and $v_2$ are calculated for a given structure according to Eq. (18).

(3) *Droplet in a very strong external field.* This case is realized when the correlation length, Eq. (5a), $\zeta\ll R$. The angle $\theta_n$ is zero nearly everywhere in a droplet and we can approximate $v_0=u$ and $v_{\pm 1}=v_{\pm 2}=0$. The resulting scattering amplitude is, as long as $\theta=0$,

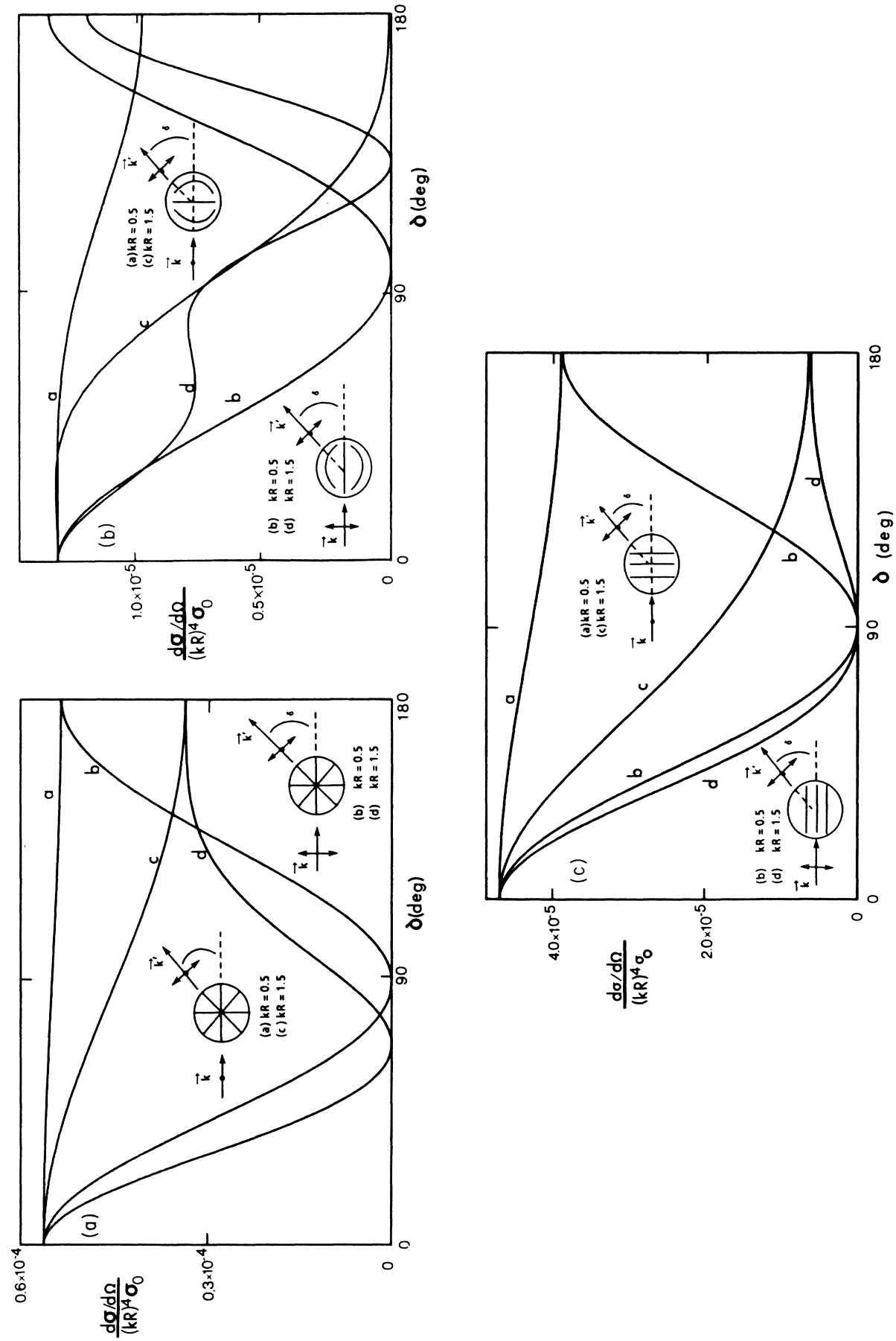


FIG. 6. Dependence of the differential cross section on the scattering angle. (a) corresponds to normal surface alignment and (b) to the tangential alignment both in zero field. The case of a very high field ($R/\xi=\infty$) is shown in (c). On all figures curve (a) represents the case $\theta=\alpha=\pi/2$ for $kR=0.5$ and curve $b$ the situation $\theta=\alpha=0$ for the same $kR$. Curve $c$ represents $kR=1.5$ with $\theta=\alpha=\pi/2$ and curve $d$ $\theta=\alpha=0$ for the same $kR$. The parameters used are $\xi=0.04$, $\eta=0.08$, and $\gamma=0$.

$$\underline{S}=\frac{(kR)^3}{3}u\begin{bmatrix}\zeta\cos\delta+\eta[(3\sin^2\theta\cos^2\gamma-1)\cos\delta-\frac{3}{2}\sin\delta\sin^2(2\theta)\cos\gamma] & \frac{1}{2}\eta[\sin\delta\sin(2\theta)\sin\gamma-\cos\delta\sin^2\theta\sin2\gamma] \\ -\frac{3}{2}\eta\sin2\gamma\sin^2\theta & \zeta+\eta(3\sin^2\theta\sin^2\gamma-1)\end{bmatrix}, \tag{44}$$

which gives us the following differential scattering cross sections:

$$\left[\frac{d\sigma}{d\Omega}\right]_{\|}=\sigma_0\frac{(kR)^4}{9\pi}u^2\{\zeta\cos\delta\cos\alpha+\eta[3\sin^2\theta\cos(\gamma+\alpha)\cos\gamma\cos\delta-\tfrac{3}{2}\sin\delta\sin(2\theta)\cos(\alpha+\gamma)-\cos\alpha\cos\delta]\}^2 \tag{45a}$$

and

$$\left[\frac{d\sigma}{d\Omega}\right]_{\perp}=\sigma_0\frac{(kR)^4}{9\pi}u^2\{\zeta\sin\alpha-\eta[3\sin^2\theta\sin\gamma\cos(\alpha+\gamma)+\sin\alpha]\}^2 . \tag{45b}$$

We will write SALS scattering intensities only for the case of $\theta=0$

$$I_{VV}(\theta=0)=\frac{R^2}{9r^2}(kR)^4u^2(\zeta-\eta)^2(1-\sin^2\delta\cos^2\alpha)^2 \tag{46a}$$

and

$$I_{VH}(\theta=0)=\frac{R^2}{9r^2}(kR)^4u^2(\zeta-\eta)^2\sin^4\frac{\delta}{2}\sin^2 2\alpha , \tag{46b}$$

where they correspond to the ones of an isotropic droplet. The total scattering cross section has the following simple angular dependence:

$$\begin{aligned}\sigma=\frac{8}{27}\sigma_0(kR)^4\{&(P_0+\tfrac{1}{2}P_2)(\zeta-\eta)^2\\&+3\eta\cos^2\alpha_0\sin^2\theta\\&\times[(2\zeta-\eta)P_0+(\zeta-4\eta)P_2]\\&+\tfrac{27}{2}\eta^2P_2\sin^4\theta\cos^2\alpha_0\} ,\end{aligned} \tag{47}$$

where $\alpha_0=\alpha+\gamma$ is the polarization angle between **k**-**N** plane and the incoming vector of the electric field **E** (see Fig. 3). The averages $P_0$ and $P_2$ are defined in the following way:

$$\begin{Bmatrix}P_0\\P_2\end{Bmatrix}=\int_0^1 u^2\begin{Bmatrix}1\\(3\cos^2\delta-1)/2\end{Bmatrix}d\cos\delta . \tag{48}$$

It is worthwhile to mention that the scattering in this case for the angle $\theta=0$ is equivalent to the scattering of an isotropic sphere[7,1] with $\epsilon_r-1=\zeta-\eta$.

## V. NUMERICAL RESULTS AND DISCUSSION

The scattered light from a nematic droplet depends on the impact angle $\theta$ and the angle of polarization $\alpha_0$ as well as on the scattering angles $\delta$ and $\gamma$. It is useful to examine some of these dependencies that are predicted by the theory, particularly as they relate to electro-optic applications where nematic droplet dispersions are utilized. In this regard we choose values of $n_\perp=1.52$ and $n_{\|}=1.70$ which are typical of cyanobiphenyl compounds known to form droplets in some polymeric materials.[16] In our choice of $n_m=1.55$ we select a value which is purposely mismatched with respect to $n_\perp$ and is also characteristic of some epoxy-type polymers.

In order to illustrate the effectiveness of nematic droplet dispersions in beam shutters, it is useful to calculate the total scattering cross section of a nematic droplet, $\sigma$, for some specific cases. Introducing $\sigma_{\rm iso}(kR)$ as the total cross section in the isotropic phase ($\eta=0$) at a specified wavelength and radius ($kR=0.1$), a plot of $\sigma/\sigma_{\rm iso}$ versus $kR$ for various director configurations and impact angles and polarizations is calculated and shown in Fig. 5. The

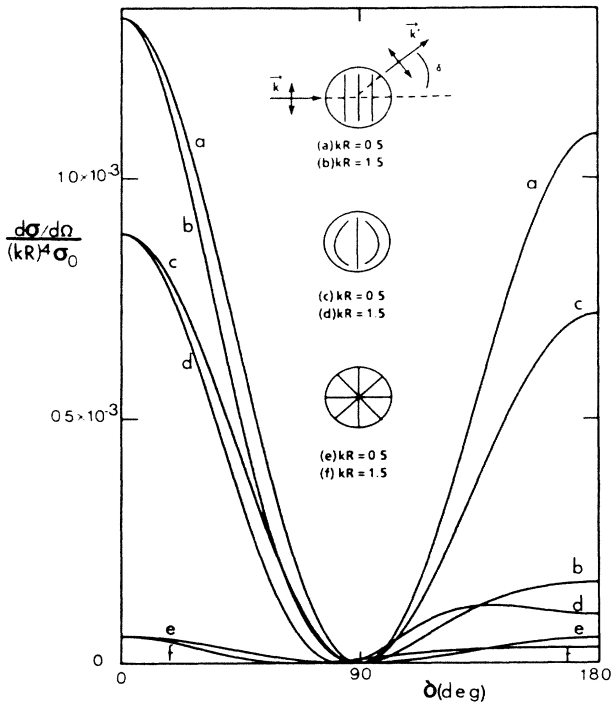


FIG. 7. The dependence of the differential cross section on the scattering angle for $\theta=\pi/2$ and $\alpha=0$ for the case of very high field ($R/\xi=\infty$) with $kR=0.5$ in curve $a$ and $kR=1.5$ in curve $b$; zero-field tangential surface alignment with $kR=0.5$ in curve $c$ and $kR=1.5$ in curve $d$; zero-field normal surface alignment with $kR=0.5$ in curve $e$ and $kR=1.5$ in curve $f$. The parameters used are $\zeta=0.04$, $\eta=0.08$, and $\gamma=0$.

log-plot illustrates the characteristic Rayleigh $\lambda^{-4}$ dependence for values of $kR \leq 2$ as well as the effectiveness of nematic droplets as light scatterers. It is seen from the plot that the radial configuration as well as the high-field case where the incident light is polarized orthogonal to the aligned directors are very nearly equivalent in their scattering power to that of an isotropic droplet. The strongest scattering [Figs. 5(a) and 5(b)] occurs with the bipolar droplet configuration and field aligned case where polarization is parallel to the direction of $n_{\|}$. The fact that plots f and g of Fig. 5 lie below the isotropic case is a reflection of the choice of $n_m$ being above the value of $n_{\perp}$.

The angular dependence of the differential scattering cross section for different director configurations, droplet sizes, and impact angles are shown in Fig. 6. We show the results for three director configurations: the radial or star configuration created from normal surface alignment at the droplet wall, Fig. 6(a); the bipolar configuration from tangential wall alignment, Fig. 6(b), and parallel director configuration from an applied field, Fig. 6(c). These figures illustrate several general features. Firstly, there appears little difference between the forward and backward scattering from small droplets whereas the difference becomes quite pronounced for large droplets ($kR \geq 1$). When the size of the droplet becomes comparable to the wavelength of light there are phase shifts in-

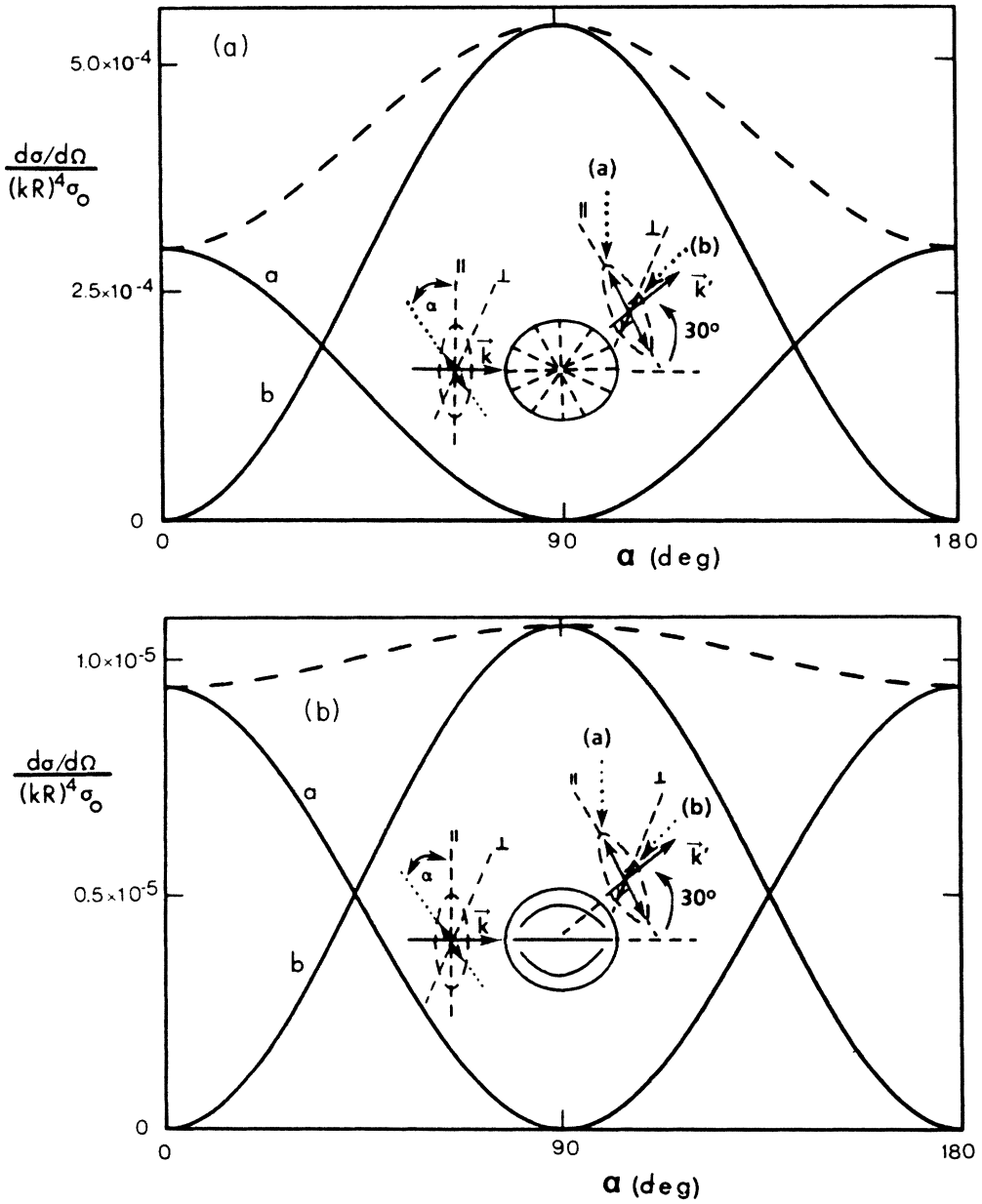


FIG. 8. Dependence of the $(d\sigma/d\Omega)_{\|}$ (curve $a$), $(d\sigma/d\Omega)_{\perp}$ (curve $b$), and of $d\sigma/d\Omega$ dashed curves on the polarization angle $\alpha$ is shown for normal surface alignment in (a) and for tangential alignment in (b). The parameters used are incident angle $\theta=0$, scattering angle $\delta=30°$, $\gamma=0$, $\zeta=0.04$, $\eta=0.08$, $R/\xi=0$, and $kR=1.5$.

side the droplet and the waves interfer to destroy the symmetry between forward and backward scattering.

Secondly, the angular dependence appears to be strongly dependent on the director configuration inside the droplet, particularly for larger droplets. This disparity between different director configurations is more pronounced at large scattering angles. These results suggest that with an independent measure of droplet size, light scattering could be used to determine the director configuration in the droplet and hence the surface alignment at the droplet wall. It is interesting to point out that the angular dependence exhibited in Fig. 6(c) is identical to the case of an isotropic droplet. In Fig. 6(c) the impact angle and polarizations are such that they give minimum scattering from the aligned droplets.

The impact angles and polarizations which give maximum scattering are those which yield the plots of Fig. 7. It is clear from this figure that droplets with a star configuration are poor scatterers compared to those of the bipolar or aligned type. Parallel surface alignment is therefore desired in droplet dispersions used in electro-optic switching devices. The symmetry between forward and backward scattering for small $kR$ is particularly evident in these plots.

The dependence of the differential cross section upon the polarization angle of the incident light is shown in Fig. 8 for a specific scattering angle. There is seen to be very little dependence of the total differential cross section, upon the polarization angle for some types of nematic configurations. It is clear from these plots that one can achieve substantially more information by measuring differential cross sections for both $\|$ and $\perp$ polarization.

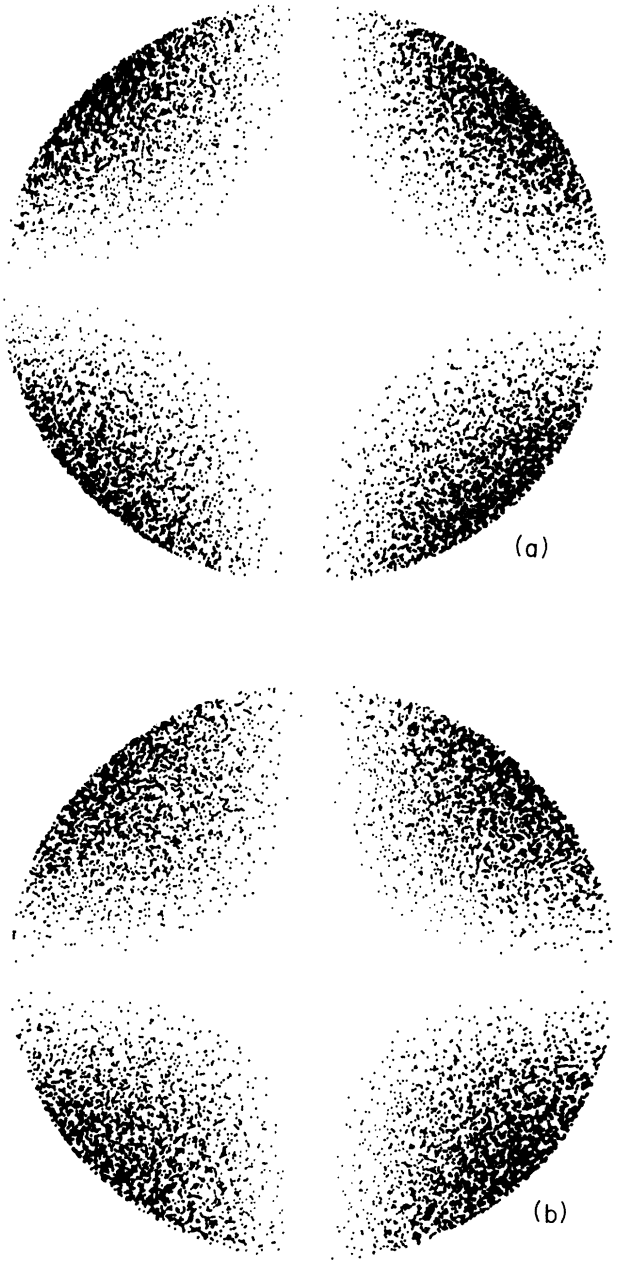


FIG. 9. Small-angle light scattering $I_{VH}$ patterns for $\theta=0$ and $\delta \leq 15°$ in case of normal (a) and tangential (b) surface alignment. The parameters used are $\zeta=0.04$, $\eta=0.08$, $R/\xi=0$, and $kR=2.0$.

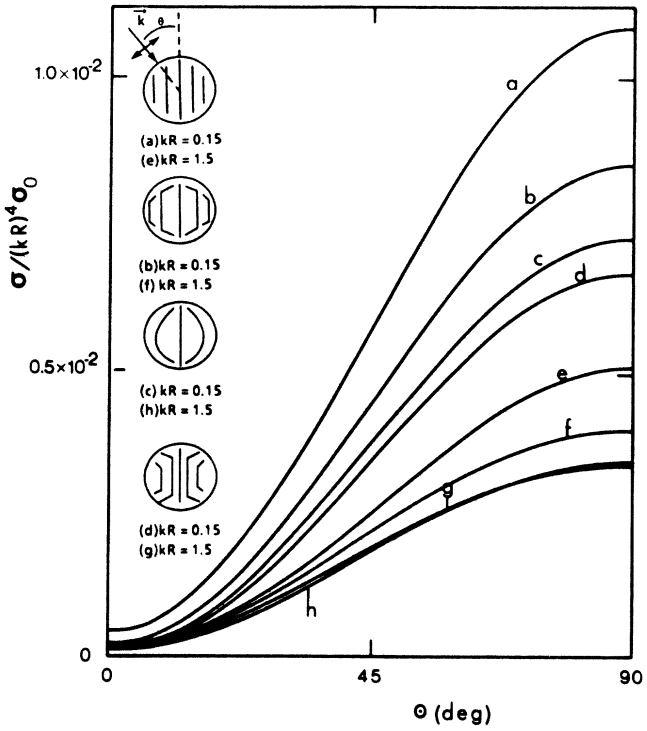


FIG. 10. Dependence of the total scattering cross section on the incident angle $\theta$ for the case of high field ($R/\xi=\infty$) with curve $a$ for $kR=0.15$ and curve $e$ for $kR=1.5$; external field where $R/\xi=5$ for tangential surface alignment represented by curve $b$ for $kR=0.15$ and curve $g$ to $kR=1.5$; zero field for tangential surface alignment with curve $c$ for $kR=0.15$ and curve $h$ for $kR=1.5$. The polarization angle $\alpha_0=0$, $\zeta=0.04$, and $\eta=0.08$ were used.

Small-angle light scattering $I_{VH}$ patterns predicted by the theory are shown in Fig. 9 for the star and bipolar configurations. The difference between these two patterns is barely noticeable suggesting that SALS scattering would not be a good method for determining director configuration inside small droplets where RGA treatment in applicable.

Important for electro-optic shutters is Fig. 10 which shows the dependence of the total scattering cross section upon the orientation of a droplet relative to the direction of incident light in various field strengths. In thin films with dispersed droplets the transparency is given by $1-N\delta$, where $N$ is the number of droplets per unit of the surface. Curves $a$ and $e$ at $\theta=0$ determine the transparency of such a film in the presence of the field (ON condition). With a perfect match between $n_m$ and $n_\perp$ there would be no scattering at all ($\sigma=0$) for this condition and the film would be perfectly transparent. Curves $c$ and $h$ give the cross section in the absence of a field (OFF condition). Normally there is a random orientation of droplets in a film. The opaqueness of the film is then determined by the help of this curve. The ratio in the total scattering cross section for the field ON and field OFF condition gives the contrast for an electro-optic shutter where the light from the shutter is collected in a small solid angle.

The effect of total cross section on the impact polarization is seen in Fig. 11 for nematic droplets in the presence of a field of intermediate strength. These curves suggest the use of nematic droplet dispersions as light polarizers. Such polarizers could be switched from a polarizing to a nonpolarizing state by application of an external field to orient the droplets.

The dependence of the total scattering cross section on refractive index of the medium $n_m$ is seen in Figs. 12 and 13. Figure 12 shows that the dependence of total cross section on the impact angle is strongly affected by the values of $n_m$. A crossover in the dependence is observed as $n_m$ is varied. Nematic droplets with normal and tangential wall alignment in the presence of a field of intermediate strength show little difference in their light scattering properties.

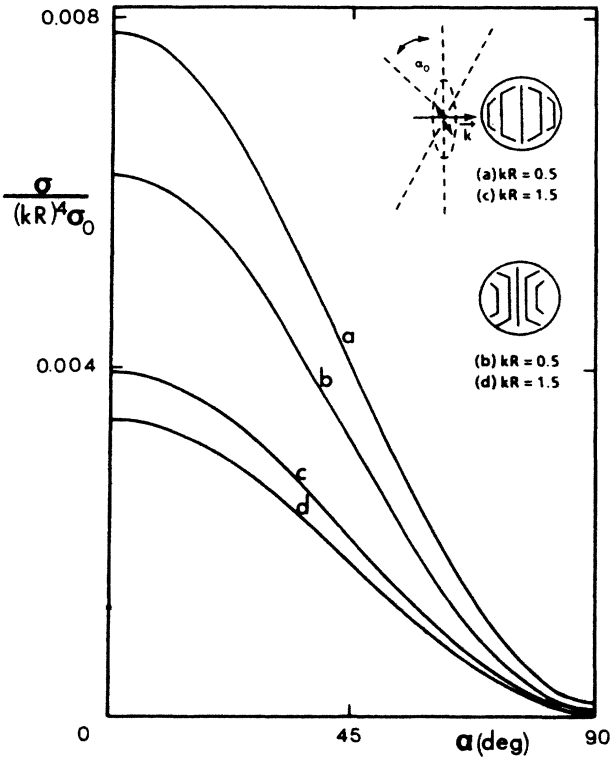


FIG. 11. Polarization dependence of the total cross section in the case of tangential surface alignment, curve $a$ for $kR=0.5$ and curve $c$ for $kR=1.5$, and in the case of normal alignment, curve $b$ for $kR=0.5$ and curve $d$ for $kR=1.5$. The other parameters are: $R/\xi=5$ (intermediate field strength) $\theta=\pi/2$, $\zeta=0.04$, and $\eta=0.08$.

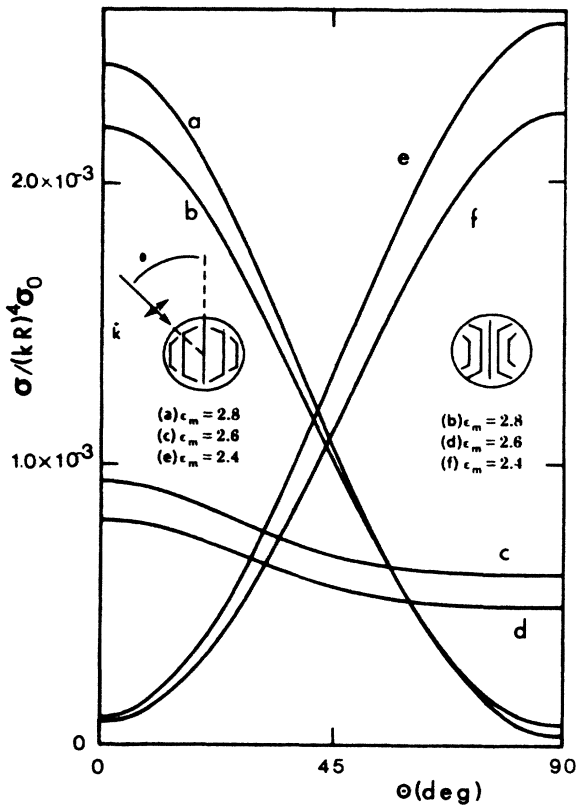


FIG. 12. Dependence of the total scattering cross section on the incident angle, $\theta$, for different surrounding medium dielectric constants: $\epsilon_m=2.8$ (curve $a$, tangential alignment; curve $b$, normal alignment); $\epsilon_m=2.6$ (curve $c$, tangential; curve $d$, normal); $\epsilon_m=2.4$ (curve $e$, tangential; curve $f$, normal). The other parameters are $R/\xi=5$ (medium strength of the external field), $\alpha_0=0$, $\zeta=0.04$, and $\eta=0.08$.

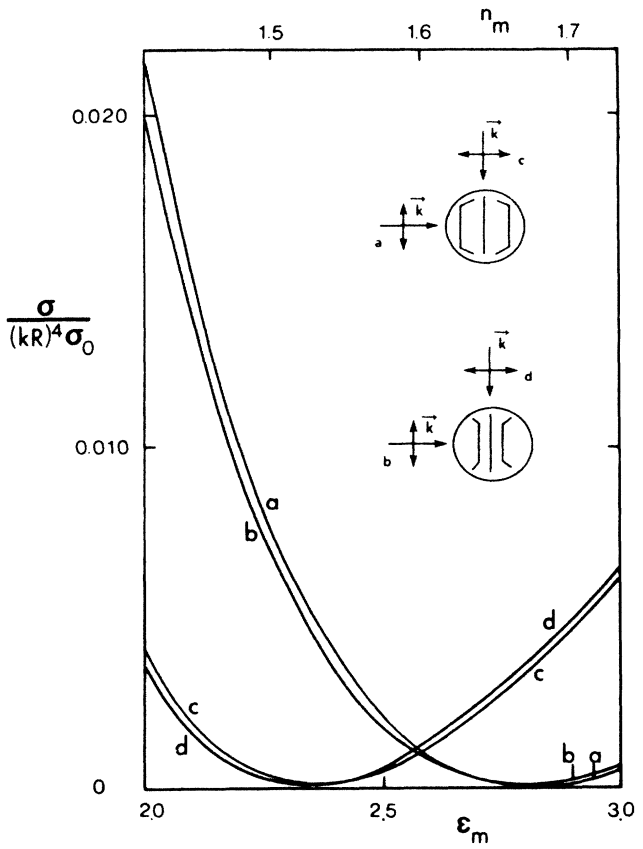


FIG. 13. Dependence of the total scattering cross section on the surrounding medium dielectric constant. Tangential surface alignment is represented by curve $a$ for the incident angle $\theta=\pi/2$ and curve $c$ for $\theta=0$. Normal surface alignment corresponds to curve $b$ for $\theta=\pi/2$ and curve $d$ for $\theta=0$. The other parameters are $R/\xi=5$ (intermediate field strength), $\alpha_0=0$, $\zeta=0.04$, and $\eta=0.08$.

Finally, Fig. 13 illustrates the role of refractive index matching. For the case where incident light is parallel to the applied field of intermediate strength [Figs. 13(c) and 13(d)] the minimum in the scattering cross section occurs at a value of $\epsilon_m=2.4$ or $n_m=(\epsilon_m)^{1/2}=1.55$. Though not illustrated, it is evident that for fields of high strength where the directors in the droplet are all aligned parallel to the direction of the field, the minimum would occur at $n_m=1.52$ which is the value used for $n_\perp$ in the numerical calculation. As in previous figures there is little difference between droplets with tangential and normal wall alignment in intermediate fields. It is interesting to note that a minimum occurs for the case where light impinges at right angles to the applied field. This minimum occurs at $n_m=(\epsilon_m)^{1/2}=1.65$ which is near the value of $n_{||}=1.70$. In electro-optic applications it is worthy to note that curves $a$ and $b$ rise more sharply than curves $c$ and $d$ as the $\epsilon_m$ is lowered below the value 2.4. This suggests that higher contrast switching might be better achieved below the minimum even though a film of droplet dispersions is less transparent in its ON condition.

## VI. CONCLUSIONS

We have presented for the first time a study of light scattering from submicron birefringent nematic droplets. The effects of various director configurations which result from different types of molecular anchoring at the wall of a spherical droplet presented. The differential scattering cross section is shown to exhibit strong dependencies on the incident and scattering angles in which different director configurations can be readily distinguished and used for the experimental study of droplet structure. The fact that these scattering effects can be controlled by an applied field introduces numerous electro-optic applications. Studies of scattering from a collection of droplets where interdroplet interference effects are taken into account are in progress.

## ACKNOWLEDGMENTS

Support by the National Science Foundation (NSF) Solid State Chemistry Program grant DMR-85-03219 is acknowledged. The authors further acknowledge M. Žumer for her assistance in the computer simulations and numerical calculations.

*On leave from the Department of Physics, E. Kardelj University of Ljubljana, YU-61111 Ljubljana, Yugoslavia.

[1]See, for instance, H. C. van de Hulst, *Light Scattering by Small Particles* (Wiley, New York, 1957).

[2]M. Kerker, *The Scattering of Light and Other Electromagnetic Radiation* (Academic, New York, 1969).

[3]C. F. Bohren and D. R. Hoffman, *Absorption and Scattering of Light by Small Particles* (Wiley, New York, 1983).

[4]G. Mie, Ann. Phys. **25**, 377 (1908).

[5]S. Asano and G. Yamamoto, App. Opt. **14**, 29 (1975).

[6]Lord Rayleigh, Philos. Mag. **41**, 107 (1871); **41**, 274 (1871); **41**, 447 (1871).

[7]R. Gans, Ann. Phys. **76**, 29 (1925).

[8]P. Debye, Ann. Phys. **46**, 809 (1915).

[9]I. O. Kulik and A. G. Shkorbatov, Opt. Spektrosk. (USSR) **51**, 701 (1981).

[10]R. S. Stein and M. B. Rhodes, J. App. Phys. **13**, 1873 (1960).

[11]M. B. Rhodes and R. S. Stein, J. Polym. Sci. A **2**, 1539 (1969).

[12]J. Roth and M. J. Digman, J. Opt. Soc. Am. **63**, 308 (1973).

[13]M. Matsuo, K. Kakei, Y. Magaoka, F. Ozaki, M. Murai, and T. Ogita, J. Chem. Phys. **75**, 5911 (1981).

[14]G. H. Meeten, Opt. Acta **29**, 759 (1982).

[15]J. V. Champion, A. Killey, and G. H. Meeten, J. Polym. Sci., Polym. Phys. Ed. **23**, 1467 (1985).

[16]J. W. Doane, N. A. Vaz, B.-G. Wu, and S. Žumer, Appl. Phys. Lett. **48**, 269 (1986).

[17]J. Fergason, SID (Society for Information Display) International Symposium Digest of Technical Papers **16**, 68 (1985).

[18]H. Kelker and R. Hatz, *Handbook of Liquid Crystals* (Verlag Chemie, Weinheim, 1980).

[19]D. W. Allender, G. L. Henderson, and D. L. Johnson, Phys. Rev. A **24**, 1086 (1981).

[20]A. J. Nicastro and P. H. Keyes, Phys. Rev. **30**, 3156 (1984).
[21]E. Dubois-Violet and O. Parody, J. Phys. C **4**, 57 (1969).
[22]M. J. Press and A. S. Arrot, Phys. Rev. Lett. **33**, 403 (1974).
[23]R. D. Williams (unpublished).
[24]P. G. de Gennes, *The Physics of Liquid Crystals* (Clarendon, Oxford, 1974).
[25]G. E. Volovik and O. D. Lavrentovich, Zh. Eksp. Teor. Fiz. **85**, 1997 (1983) [Sov. Phys.—JETP **58**, 1159 (1983)].
[26]J. A. Stratton, *Electromagnetic Theory* (McGraw-Hill, New York, 1941).
[27]A. Ishimaru, *Wave Propagation and Scattering in Random Media,* Vol. 1 of *Single Scattering and Transport Theory* (Academic, New York, 1978).
[28]C. Acquista, Appl. Opt. **15**, 2932 (1976).
[29]R. M. Drake and J. E. Gordon, Am. J. Phys. **53**, 955 (1985).
[30]A. Plaza and R. S. Stein, J. Polym. Sci. **40**, 267 (1959).